

## Supplementary Materials

# Effect of Oxygen Annealing Atmosphere on Structural, Electrical and Energy Storage Properties of $\text{Bi}_{0.5}\text{Na}_{0.5}\text{TiO}_3$ Polycrystalline Thin Film

Ilham Hamdi Alaoui, Nathalie Lemée, Françoise Le Marrec, Moussa Mebarki, Anna Cantaluppi, Delphine Favry and Abdelilah Lahmar \*

Laboratory of condensed Matter Physics, University of Picardie Jules Verne, 33 Rue Saint Leu, 80039 Amiens, France;

\* Correspondence: abdelilah.lahmar@u-picardie.fr; Tel.: +33-3-22-82-76-91

## 1. Microstructural analysis

Scanning microscopy (SEM) micrographs of thin BNT films annealed at 600 °C under different atmospheres are shown in Figure S1. It is worth noting that BNT films annealed under oxygen, exhibits a relatively dense grained structure without electron porosity and cracks. In addition, grains seems to be uniformly distributed (Figure.S1a). However, the films annealed under  $\text{N}_2$  (BNT- $\text{N}_2$ ) (Figure.S1b) show sponge like microstructure similarly to what is reported by Yang et al.[1] for  $\text{Na}_{0.51}\text{Bi}_{0.50}(\text{Ti}_{0.96}\text{W}_{0.01}\text{Ni}_{0.03})\text{O}_3$  thin films. The authors showed that the microstructure is governed by Na nonstoichiometry. Such sponge microstructure is observed for the composition with high oxygen vacancy concentration and larger grain size. Finally, for the films annealed under Argon (BNT-Ar) (Figure.S1c), the microstructure consists of equiaxed grains with some scattered pores but are rather dense and smooth across the full sample, in good agreement with typical microstructure reported in the literature for BNT thin films prepared by CSD [2]. A typical cross-section of the films annealed under  $\text{O}_2$  (BNT- $\text{O}_2$ ), is presented in Figure S1d. It evidences a uniform thickness of about 475.6 nm (note that no significant influence of the annealing atmosphere on the films thickness was observed).

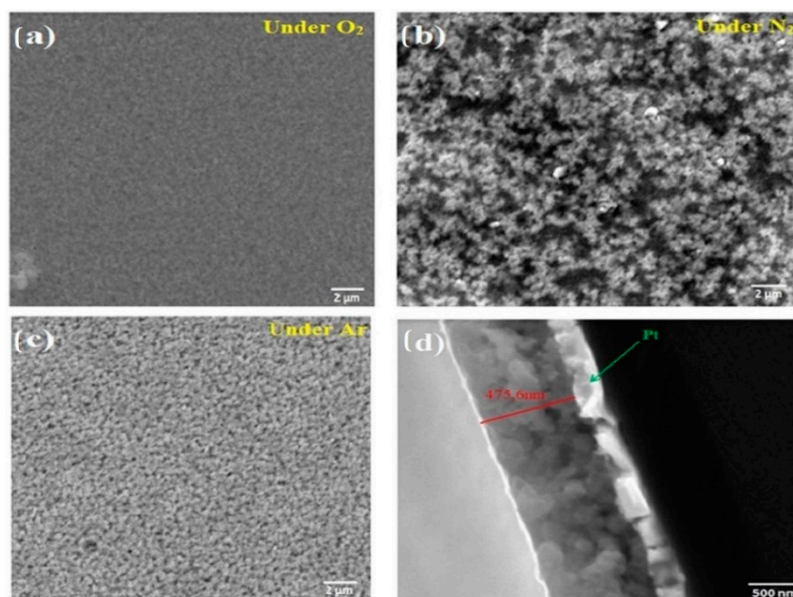


Figure S1. SEM images showing the microstructure of BNT thin films annealed at 600 °C under different atmospheres (a) O<sub>2</sub>, (b) N<sub>2</sub> and (c) Ar, (d) Example of cross-sectional image of the BNT thin film annealed under O<sub>2</sub>.

Figure S2 presents the EDX spectra in compositional distribution for the investigated BNT films. As expected, characteristics of starting elements, namely Bi, Na, Ti and O, are detected. A close look to the obtained atomic weight reveals that the BNT films annealed under O<sub>2</sub> (BNT-O<sub>2</sub>; Figure S2a) or Ar (BNT-Ar; Figure S2b) atmosphere show deficiency of Na atoms compared to the samples annealed under N<sub>2</sub> (BNT-N<sub>2</sub>; Figure S2c).

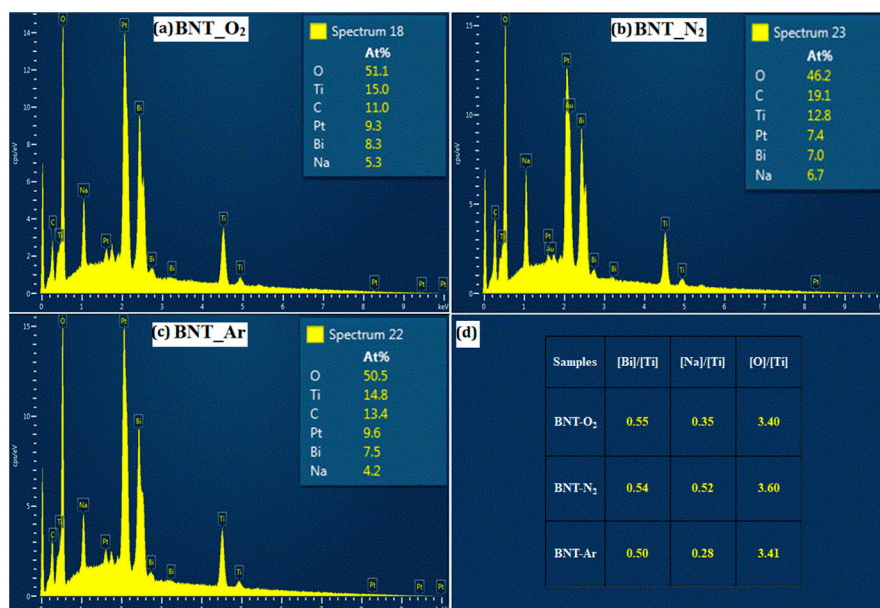


Figure S2. EDX spectra with elemental composition of BNT thin films annealed under O<sub>2</sub>, N<sub>2</sub>, and Ar atmospheres

The surface topography and roughness investigated by AFM provide more insight into the understanding of the microstructure. The topography of the film surfaces obtained in contact mode AFM is shown in Figure S3. The images were recorded on the 10 × 10 μm<sup>2</sup> scan regions. A fine-grained structure is observed for all samples which are essentially smooth. Nevertheless, if we look more closely the 2D and 3D AFM images, we can notice that the grains are larger for the films treated under N<sub>2</sub> and Ar. This result is confirmed by the root mean square (RMS) roughness whose value around 1.5 nm for the film treated under O<sub>2</sub> atmosphere, increases by a factor of two for the film treated under N<sub>2</sub> (Rms ~3.9 nm) or under Ar (Rms ~2.9 nm). This clearly demonstrates that the microstructure is affected by the nature of the gas atmosphere.

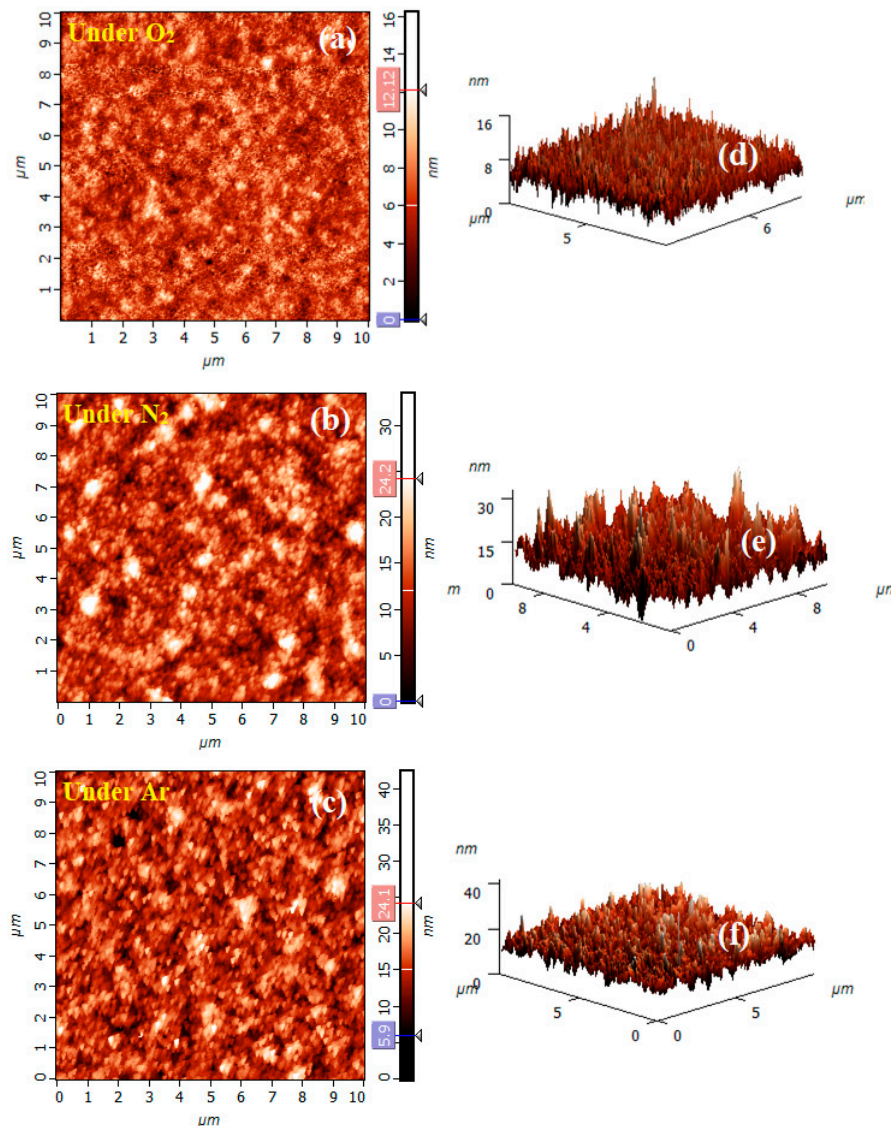


Figure S3. (a, b and c) AFM micrographs of the BNT thin films deposited by the Sol gel method on a Pt/SiN substrate under the atmospheres of oxygen, nitrogen and argon, respectively; and (d, e and f) the corresponding 3D AFM images, respectively.

## 2. Structural investigations

The XRD patterns of the investigated samples are shown in Figure S4. The grazing incidence mode (GI) was used to eliminate the substrate contribution. Both films annealed under N<sub>2</sub> and Ar showed the presence of peaks of BNT perovskite in addition to the peaks of the secondary phase. The obtained diffraction peaks of Au are coming from the top electrodes deposited for electrical measurements. Only the film annealed under O<sub>2</sub> leads to a pure BNT perovskite.

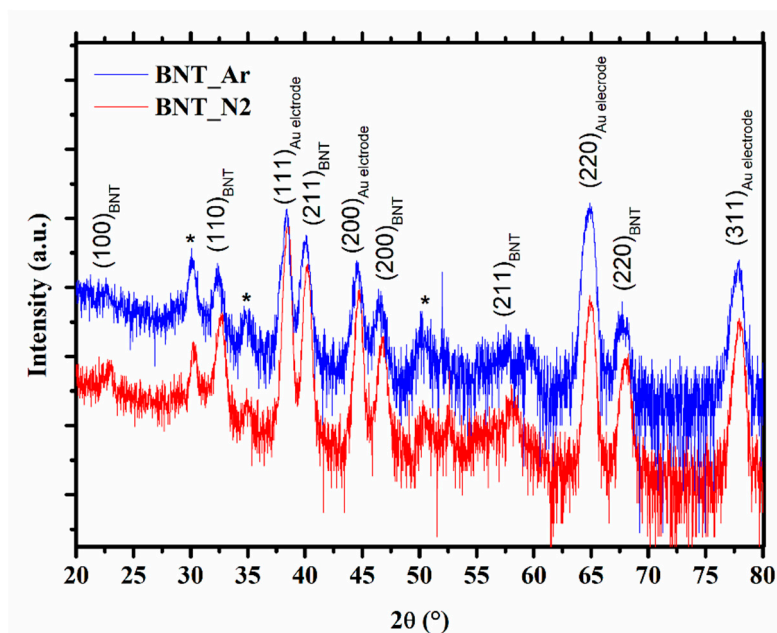


Figure S4. Room-temperature x-ray diffractogram of BNT thin films annealed under N<sub>2</sub> and Ar atmospheres.

Raman spectroscopy is used in the present work as a powerful tool to get complementary information about the structural changes, which are not accessible by XRD technique. The room temperature spectra of the investigated films are presented in Figure S5, together with the Raman spectrum of a BNT ceramic given for comparison.

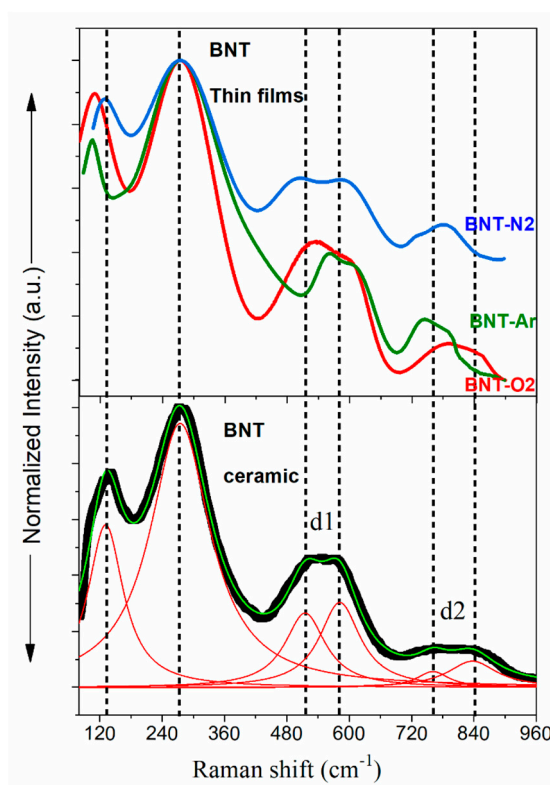




Figure S5. Comparison of the room temperature Raman spectra of the BNT thin films annealed under different atmosphere. The spectrum of a BNT ceramic is given as reference.

The comparison of the Raman spectra presented in the figure 5 shows that for all samples no change in position is detected for the intense band assigned to the Ti-O vibration at  $275\text{ cm}^{-1}$  as in the bulk ceramic. However, the lower mode corresponding to the Na-O vibration exhibits a downward shift for both BNT-O<sub>2</sub> and BNT-Ar films. The shift of this mode towards lower frequencies could be attributed to the Na<sup>+</sup> deficiency.

### 3. Ferroelectric properties

Figure S6 shows the ferroelectric properties at room temperature for both BNT-N<sub>2</sub> and BNT-Ar samples. Only, a leaky hysteresis loops are obtained for both BNT-N<sub>2</sub> and BNT-Ar.

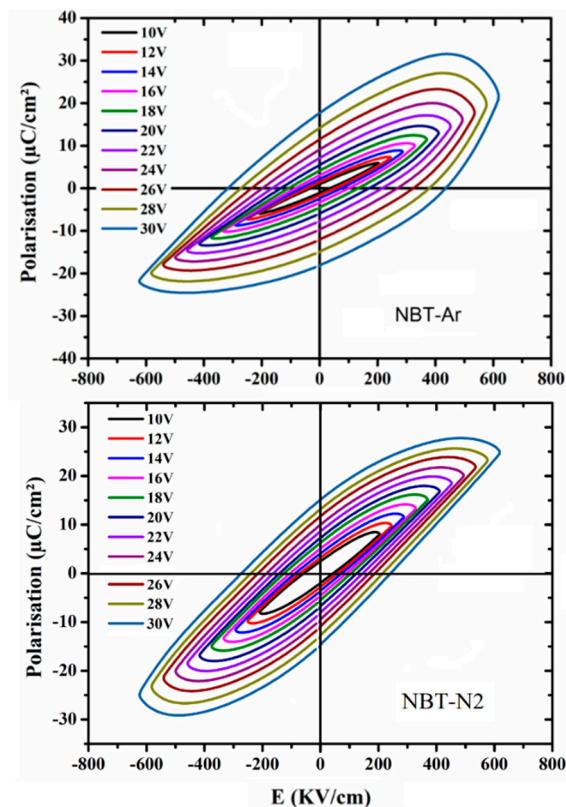


Figure S6. P-E hysteresis loop of BNT thin films prepared under Ar and N<sub>2</sub> atmosphere, respectively.

### References

1. Yang CH, Yao Q, Qian J, et al (2018) Growth, microstructure, energy-storage and dielectric performances of chemical-solution NBT-based thin films: Effect of sodium nonstoichiometry. *Ceramics International* 44:9152–9158. <https://doi.org/10.1016/j.ceramint.2018.02.123>
2. Zannen M, Belhadi J, Benyoussef M, et al (2019) Electrostatic energy storage in antiferroelectric like perovskite. *Superlattices and Microstructures* 127:43–48. <https://doi.org/10.1016/j.spmi.2018.03.041>